Hobby-Eberly Telescope low-resolution spectrograph J-band camera

Tufts, Joseph, Wolf, Marsha, Hill, Gary

Joseph R. Tufts, Marsha J. Wolf, Gary J. Hill, "Hobby-Eberly Telescope low-resolution spectrograph J-band camera," Proc. SPIE 4008, Optical and IR Telescope Instrumentation and Detectors, (16 August 2000); doi: 10.1117/12.395531

SPIE.

Event: Astronomical Telescopes and Instrumentation, 2000, Munich, Germany

Hobby-Eberly telescope low-resolution spectrograph J-band camera

Joseph R. Tufts[a], Marsha J. Wolf[a], and Gary J. Hill[b]

[a]University of Texas at Austin, Department of Astronomy, C-1400, Austin, TX 78712 USA

[b]University of Texas at Austin, McDonald Observatory, C-1402, Austin, TX 78712 USA

ABSTRACT

This paper presents the design of a near infrared camera for the 9.2 m Hobby-Eberly Telescope (HET) Low Resolution Spectrograph (LRS), which will cover the wavelength range 0.85 to 1.35 μm. The LRS-J, an upgrade to the existing LRS, replaces the optical camera with an $f/1$ camera optimized for the J-band. The instrument design is strongly motivated by the desire to observe galaxies at $1 < z < 2$, where the principal strong spectral features used to measure redshifts are shifted into the J-band. Since we are primarily interested in wavelengths up to 1.35 μm, mating the cryogenically cooled camera to the warm LRS spectrograph does not result in enough thermal background emission to compromise its performance. LRS-J represents a rapid and cost-effective way to enable multi-object near-IR spectroscopy on a very large telescope.

The camera will use a HAWAII 1024 × 1024 HgCdTe detector array in a dewar cooled by a closed cycle helium refrigerator. A novel feature of instrument is the use of large Volume Holographic (VH) grisms. VH gratings have attracted a great deal of interest recently because of their high efficiency, but they are particularly useful in the near infrared, where their efficiencies approach $\sim$ 90%. We will demonstrate the use of large (160 mm diameter) VH grisms as a retro-fit to the LRS grism spectrograph, and in the process achieve peak efficiencies in the J-band which approach 25% on the sky. The complete spectral range will be covered by 2 grisms, resulting in an instrument resolution of $R = 1400 - 2400$. The successful application of VH grisms to the LRS will open up many possibilities for retro-fitting other spectrographs to be more flexible and efficient.

Keywords: Astronomical instrumentation: spectrographs, HET Low Resolution Spectrograph, infrared, volume holographic grism; Detectors: HgCdTe; Telescopes: Hobby-Eberly

1. INTRODUCTION

The J-band extension to the Hobby-Eberly Telescope's (HET)[1] low-resolution spectrograph (LRS),[2] which we call LRS-J, is primarily motivated by the desire to observe galaxies at $1 < z < 2$. This redshift regime is extremely important for studies of galaxy evolution, since galaxies at lower redshifts appear quite similar to those around us, but at redshifts $z > 2$ they have clumpy, irregular structure and may be undergoing mergers at a high rate. Unfortunately, these galaxies' principal strong spectral features, which are used to determine redshift, are shifted into the J-band, beyond the sensitivity of CCD detectors. In this wavelength region HgCdTe detectors have QE > 50%, and with such detectors it becomes relatively straight-forward to obtain redshifts of L* galaxies (at the knee of the luminosity function) in 1 hour integrations on the HET. Hence, important strides in our understanding of galaxy evolution can be made using our relatively simple LRS-J camera in conjunction with the LRS spectrograph in its multi-object mode.

LRS-J is a simple upgrade to the existing LRS as it essentially replaces the optical camera with one optimized for the J-band. Since we are primarily interested in wavelengths short of 1.35 μm, mating the camera to the warm LRS spectrograph will not compromise its performance. On the contrary, due to the thermal background, it would not be possible to extend coverage to the H-band.[3,4] Fortunately, the science focus of the instrument is well served by observations exclusively in the J-band. Furthermore, the multi-object unit has 13 remotely configurable slitlets

Further author information:
J.R.T. Email: grin@astro.as.utexas.edu
M.J.W. Email: mwolf@astro.as.utexas.edu
G.J.H. Email: hill@astro.as.utexas.edu

In *Optical and IR Telescope Instrumentation and Detectors*, Masanori Iye, Alan F. M. Moorwood, Editors, Proceedings of SPIE Vol. 4008 (2000) • 0277-786X/00/$15.00

giving a very flexible system that can be reconfigured on the fly. Consequently LRS-J represents a straight forward and cost-effective way to enable multi-object near-IR spectroscopy on one of the world's largest telescopes.

The LRS-J will have three observing modes covering the 0.85 to 1.35 μm wavelength region: imaging over the 4 arcmin diameter FOV of the HET in z and J bands; longslit spectroscopy with slit widths $\geq$ 1.0 arcsec; and multi-object spectroscopy (MOS) of up to 13 objects at a time with 1.3 $\times$ 15 arcsec slitlets on 20 arcsec centers.

In MOS mode, the exposures will be $\sim$ 10 minutes and the telescope will be nodded between two positions $\sim$ 5 arcsec apart along the slitlet direction between exposures to provide good sky subtraction. In longslit mode the nodding distance can be larger, but 5 arcsec is adequate with the expected 1–1.5 arcsec images once the segment alignment maintenance system (SAMS)[1] is installed on the HET. As with the optical LRS we will use the imaging mode for field acquisition and setup. Once the LRS-J camera and grisms are delivered, we will be able to rapidly extend our surveys in redshift with a minimum of new software and procedures.

With the LRS-J we also demonstrate the use of large (160 mm diameter) VH grisms as a retro-fit to the LRS grism spectrograph, and in the process achieve peak efficiencies in the J-band which approach 25% on the sky. Furthermore, from an instrument design perspective, the successful application of VH grisms to the LRS will open up many possibilities for retro-fitting other spectrographs making them more flexible and efficient.

2. TELESCOPE AND SPECTROGRAPH

Owing to the rather unusual design of the HET, the LRS, mounted in the telescope's central obstruction, is an integral part of the HET design. We will briefly review the HET and LRS so the reader is more familiar with the constraints their designs place on the implementation of LRS-J.

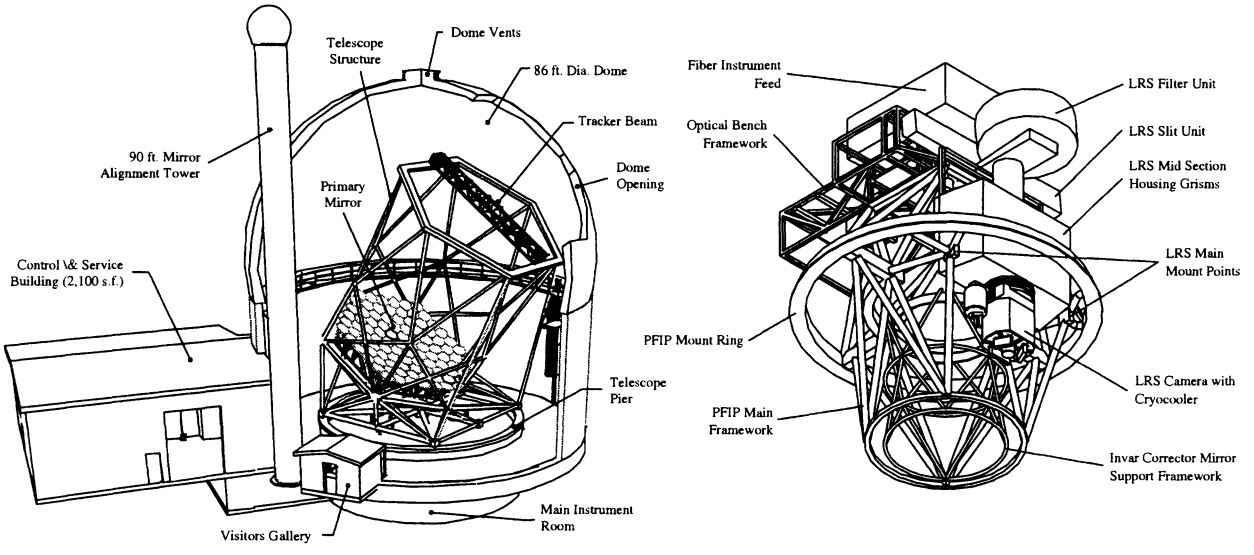

Figure 1. The HET and the prime focus instrument package (PFIP). The 11 foot tall PFIP which rides atop the tracker beam is home to the LRS. The LRS-J camera and cryogenic cooling system substitutes for the LRS camera and cryocooler.

2.1. Hobby-Eberly Telescope

The HET (Fig. 1) is a unique large telescope, based on the tilted-Arecibo concept, that sits at a fixed zenith angle of 35°. Its 11 m hexagonal-shaped spherical primary is composed of 91 hexagonal Zerodur^{TM} segments each 1 m in diameter. It can be moved in azimuth to access approximately 70% of the sky visible at McDonald Observatory in west Texas.[5,6]

The pupil is 9.2 m in diameter, and sweeps over the fixed primary as the $x-y$ tracker follows objects for between 40 minutes (in the south at $\delta = -10.3°$) and 2.8 hours (in the north at $\delta = +71.6°$). The maximum track time, per night, on a single field is 5.6 hours and occurs at $\delta = +63°$. These times are quoted for an effective 8 m aperture

since the pupil partially falls off the mirror near the extremes of the tracks. The HET was dedicated on Oct. 8, 1997, and is now in early science operations, following the delivery of the Low Resolution Spectrograph (LRS), the first facility instrument, in April 1999. The HET optics are silver-coated (Denton Vacuum FS99^{TM} enhanced silver) and, as a result, the telescope's throughput drops rapidly below 400 nm, but it has excellent efficiency in the red and near-IR. HET is a collaboration of the University of Texas at Austin, Pennsylvania State University, Stanford, Georg-August-Universität, Göttingen, and Ludwig-Maximillians-Universität, Munich. The Marcario Low Resolution Spectrograph is a joint project of the Hobby-Eberly Telescope partnership and the Instituto de Astronomia de la Universidad Nacional Autonoma de Mexico.

The LRS rides in the Prime Focus Instrument Package (PFIP, Fig. 1) on the tracker, allowing it to image as well as take spectra. The remaining facility instruments, the Medium Resolution Spectrograph[7] and High Resolution Spectrograph,[8] are located in the spectrometer room under the telescope, internal to the pier. They are fed by fibers from the fiber instrument feed on the PFIP.

The final remaining commissioning obstacle, the thermally driven de-stack of the primary mirror segments, will be overcome with the Segment Alignment Maintenance System (SAMS) edge-sensor project. At that point the HET will deliver 1 arcsec images in good seeing and acquire data 100% of the night.[1] The SAMS project is scheduled for completion in 2001.

2.2. Low-Resolution Spectrograph

The LRS is a robust instrument with high throughput in order to take advantage of the limited track time available on any one source (Sect. 2.1). Though the PFIP rotates about the corrector axis in order to access different position angles, during a typical track the rotation will change by a maximum of 15° when pointed north. Furthermore, the HET sits at a fixed 35° from the zenith, so there is nearly a constant gravity load along the axis of the LRS. As a result, flexure during a track is not a concern; a situation comparable to that for a Nasmyth mounted instrument.

The physical constraints of the PFIP dictated that the LRS design be linear with a fold, so a refractive collimator and grism disperser were adopted.[9] The refractive collimator of the LRS consists of a doublet and a triplet. The triplet is translated axially to focus the instrument. A mirror folds the collimator to conform to the space envelope. The space between the collimator triplet and the camera is 330 mm to allow room for even the largest echelle grisms. Two grisms can be carried in the LRS at any one time, and are inserted into the beam against hard stops by pneumatic cylinders.[10] The camera is an integral unit which includes the CCD head and cryocooler. Since the camera accepts the collimated beam, making its alignment with the rest of the instrument non-critical, removing it for maintenance or swapping it for the IR camera is straight-forward.

The optical camera is an $f/1.4$ catadioptric with all spherical surfaces. For the LRS, this design is preferred over a refractive design due to the required fast focal ratio, the ability to tolerate a central obstruction, and the relatively low cost. Analysis of the throughput of suitable (but slower) refractive designs indicated that when glass transmission and reflection losses are considered, a refractive camera would have only a minor throughput advantage, at best.

The LRS has been designed from the start with the aim of extending coverage to 1.35 μm, only requiring the exchange of the camera, grisms and filters. Grism and filter exchanges are trivial, and we expect to be able to exchange the cameras with only a 24 hour cycle time (due primarily to the 12-14 hour time for the cryostats to warm to ambient so the gas lines of the cryocoolers can be disconnected).

2.3. Multi-Object Spectroscopy Unit (MOS)

This remotely configurable unit is significantly more complicated than the usual method of mounting punched or etched slit-masks in an instrument. Despite this, the flexible design of the MOS unit is necessitated both by its remote location and the queue-scheduling of the HET.

The MOS unit has 13 independent fused-silica slitlets mounted on precision miniature cross-roller ways and moved by miniature geared stepper motors with lead screws. Presently mounted slits are each 1.3 arcsec wide by 15 arcsec long and spaced on 19.6 arcsec (4 mm) centers. The gaps between slit substrates are covered by thin invar sheet masks. We have achieved 1–2% width variation for the 1.3 arcsec (300 μm) wide slits, which are themselves AR coated with MgF_2. The coating also serves as a protective layer and does not cut down on red transmission. Unfortunately, no scheme could be developed that would allow variable slit width within the space constraints (the focal plane is only 50 mm in size), but the chosen solution is certainly robust and repeatable.

On any given night, a number of multi-object projects may be executed, and management of the instrument setup to allow for all the possibilities is a daunting task. Therefore, the MOS unit can be configured in less than 5 minutes, allowing scientists to adjust slitlet coordinates up to the time of the observation (a web-based MOS setup package has already been written to allow this if necessary). This level of flexibility would be impossible with masks.

For a more detailed explanation of this instrument, the reader is referred to a paper by Wolf, et.al. in these same proceedings.[11]

3. DESIGN CONSIDERATIONS

Until recently the small format of IR detectors forced observations requiring significant wavelength coverage to be made at low resolution or pieced together from many individual observations. Poor read-noise also limited detector sensitivity and thus resolution for faint objects. The current generation of detectors has both large format and low read-noise. Consequently, resolution can be increased reducing the fraction of pixels seeing OH^- emission lines, further increasing the signal-to-noise ratio (S/N).

3.1. Optimal Resolution

The sky background at $\lambda < 1.8\,\mu$m is dominated by strong OH^- emission lines, but there is also a significant background between the OH^- lines, that would amount to several hundred photons per second per micron for the aperture of the HET.[12,13] As a result, increased spectral resolution allows a larger fraction of resolution elements to see a lower background, and it becomes possible to detect faint objects if the read-noise of the detector is low. There is, however, a limit to how high a resolution is effective.

Keith Thompson has analyzed the advantages of higher resolution,[13] and he kindly ran some simulations of the LRS in the J-band to define an optimum resolution for the instrument. We considered 1.0 and 1.5 arcsec wide slits and a variety of dispersions, for a total integration time of 3600s. When the galaxy spectral features we are interested in are resolved, the advantages of higher resolution begin to diminish. We found that most of the advantage of higher resolution is had by $R \sim 2300$. There is very little gain in doubling the resolution from there. On the other hand there is a significant gain between $R \sim 1000$ and $R \sim 2300$ where average noise is decrease by 30% for a 1 hour integration. So we conclude that the optimum resolution is $R \sim 2000$, but that $R \sim 1600$ is adequate to reach faint limits for the majority of the pixels.

When SAMS is installed, image quality will increase dramatically, but will still only deliver 1 arcsec images under the best conditions. For this reason we have chosen 1.3 arcsec slits for the MOS. These represent a safe estimate of average image quality once SAMS is installed.

The limiting magnitude between the OH^- lines is relatively insensitive to resolution for $1000 < R < 2500$, and is $J \approx 22$ for 1 hour integrations, but the fraction of pixels affected by OH^- emission (and hence having higher noise) decreases with increasing resolution. The higher resolutions are not needed below $\lambda \sim 1\,\mu$m where the OH^- lines are much weaker and $R \sim 1000$ is adequate.

3.2. Detector Choice

To make full use of the multi-object advantage and to get adequate wavelength coverage at high enough resolution, a large format detector is necessary. Since we are focusing on the J-band and wish to keep the instrument as simple as possible, HgCdTe detectors rather than InSb are favored despite the QE advantage of InSb (90% vs. 50%) and the residual memory effects in the dark count of HgCdTe arrays. We will minimize the residual memory effect, which decays with an exponential time-constant of about 50 s, following significant saturation on bright objects, by reading the array for 2 minutes prior to starting a spectroscopic integration. We will save the data accumulated during this time as a record of any residual images.

The large format HgCdTe options are the Rockwell HAWAII array ($1024^2 \times 18.5\,\mu$m pixels)[14] or the HAWAII-2 array ($2048^2 \times 18\,\mu$m pixels).[15] Since the 4 arcmin diameter HET field-of-view can be made to fit easily on either chip, the choice is primarily driven by wavelength coverage at the desired resolution. For the HAWAII-2 array, a camera design very similar to the optical one at $f/1.4$ could be used. It would yield 0.3 arcsec/pxl with wavelength coverage, at $R \approx 2300$, of 0.85 to 1.35 μm in two overlapping exposures. In order to use the HAWAII array, a faster camera is needed. Note that Rockwell HgCdTe arrays have a sapphire layer ($n = 1.77$) which is bonded to the HgCdTe

($n = 3.5$). We have analyzed the reflectivity of this combination and find total reflection at $\approx 57^o$ ($f/0.65$). On the other hand the 45^o incidence present in an $f/1$ system has reflection of 12% compared to 15% at normal incidence.

The original LRS camera is a Cuevas-Maksutov variant designed at IAUNAM (Mexico City) by F. Cobos and C. Tejada.[9] We have investigated how fast this design can be pushed for a chip the size of the HAWAII array, and have reached a limit at $\sim f/1$. Such a camera is possible, but $f/0.7$ (to give the same wavelength coverage as for the HAWAII-2 array) is not.

Sacrificing some wavelength coverage the $f/1$ performs well (Sect. 4), and the tolerance analysis confirms that the relative insensitivity of the slower optical camera to alignment errors is preserved in the faster design.With this design, at $f/1$, the HAWAII array would have 0.42 arcsec/pxl, providing good sampling of the 1–1.5 arcsec images of the HET.

The primary advantages of the HAWAII array over the larger HAWAII-2 array are significantly lower cost ($250K less, including the electronics, see Sect. 6 for details), immediate availability, and significantly lower obstruction of the detector head assembly which sits in the light beam within the camera. The HAWAII-2 ZIF socket and chip carrier are bulky and our exploratory layouts show that the detector head would present a $\sim 40\%$ areal obstruction, while the HAWAII array package would fall mostly within the 28% central obstruction of the HET.

The resolution arguments presented above do seem to argue for the larger detector, with the trade-off being one of wavelength coverage: at a given resolution the HAWAII array at $f/1$ covers 66% of the wavelength range of the larger detector. However, the smaller obstruction of the HAWAII array results in 25% higher throughput for the instrument, indicating the HAWAII array would require only ~ 1.6 times the integration time to get the same resolution and wavelength coverage). Given the above arguments, we feel that the practical advantages of the HAWAII array outweigh the ~ 1.5 larger wavelength coverage that the HAWAII-2 array would deliver at the same resolution, thus our design is developed around the smaller detector.

3.3. Thermal Background

The camera in this instrument will be cooled, but the existing LRS will not. Since the detector will see a grism and other optics at ambient temperature with an emissivity, $\epsilon \approx 1$, the thermal background limit becomes important for high resolution observations, even in the J-band. The desire is to keep the thermal background shot noise in typical exposures below the read noise of the detector, which is expected, with multiple reads, to be $6\,e^-$/pixel on the HAWAII array. The thermal background rate, in e^-/sec/pixel, is calculated with the equation,

$$\dot{N} = 2cA\Omega \int_{\lambda_1}^{\lambda_2} \eta F \lambda^{-4} \exp\left(1 - \frac{hc}{\lambda kT}\right) d\lambda$$

where c is the speed of light, A is the pixel area (18.5 μm pixels), Ω is the solid angle at which a pixel sees the ambient background (0.66 str for $f/1$), η is the efficiency of the detector and cold optics (0.5 assumed), F is the cold filter transmission (unity assumed), and T is the ambient site temperature (283 K (50^oF) assumed). With the long wavelength cutoff, $\lambda_2 = 1.35\,\mu$m, the thermal background noise, $\sqrt{N}$, in a five minute integration is 5 electrons. This significantly below the expected sky background between OH^- emission lines.

For $R = 2300$ the noise floor per pixel is about 30 e^- in an hour integration, compared to 17 e^- in the thermal component, so the thermal background is negligible compared to the ambient background at all wavelengths in the J band. The same is true in the z band. Hence the design will provide background limited performance at $R = 2300$ in the z and J bands, and coverage to 1.35 μm. This is not the case in the H band, however, so we do not intend to extend coverage to longer wavelengths, which would compromise performance at all wavelengths.

4. OPTICAL DESIGN

LRS-J optical design is composed of two separate components: the camera's imaging optics and the spectrograph's dispersing optics (VH grisms). We chose this design plan to demonstrate that it would be possible to retrofit other grism spectrographs with efficient VH dispersion elements.

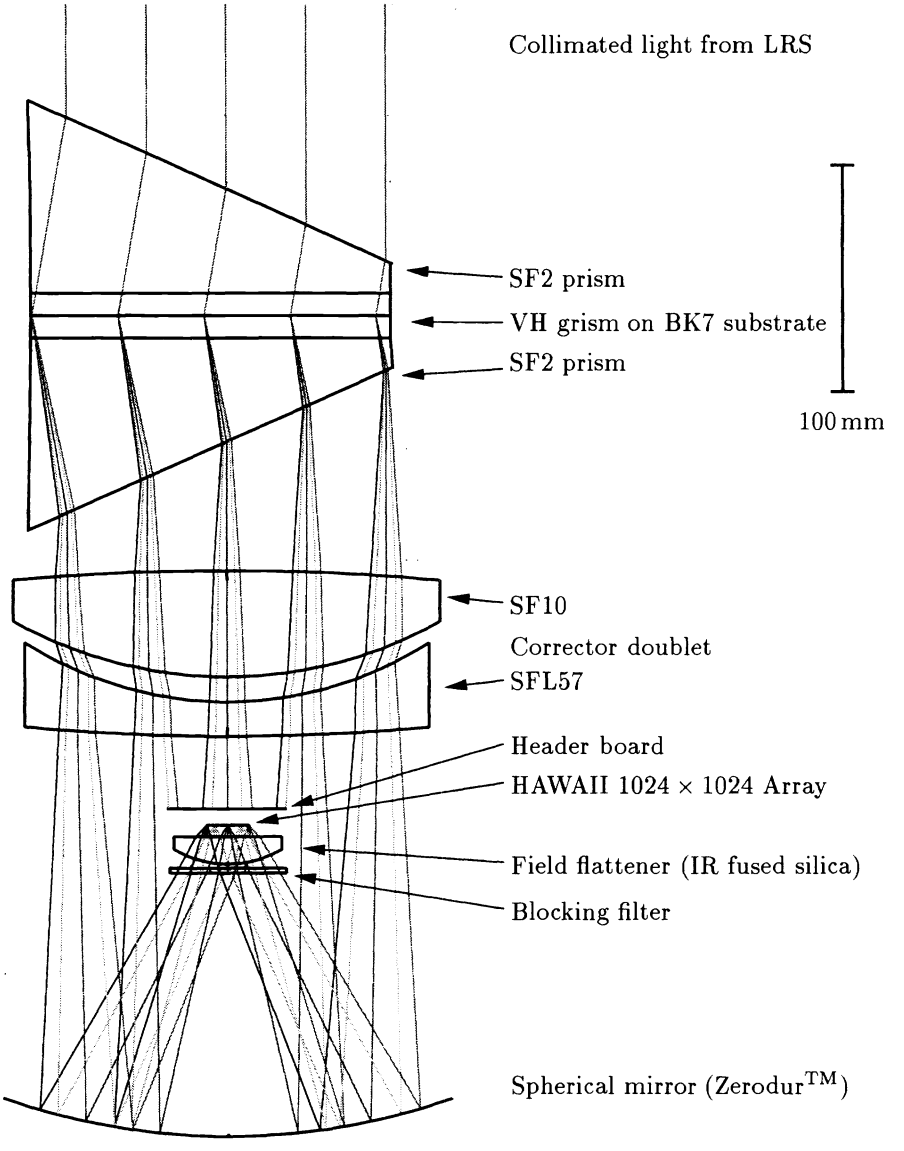

Figure 2. Preliminary design of the LRS-J band camera. Collimated light enters the grism from the top.

4.1. Imaging Optics

The optical design of the LRS-J camera is based on the successful design of the existing LRS camera, and has been optimized by the same designers (Sect. 7). The camera is composed of all spherical elements as indicated in Fig. 2. For reference, the large optics are 185 mm diameter, and the pupil is 142 mm diameter. The physical spacing between the negative corrector lens and the backside of the detector is 50 mm, adequate space for electronics. This space will be adjusted in conjunction with the header board design (Sect. 6.1) but will not need to be increased.

The larger, outer biconvex element of the corrector doublet will serve as the cryostat window, and we will design it to include the deflection caused by the pressure difference across it (Sect. 5.2). The last elements before the chip are a planar blocking filter designed to cut off sharply at 1.35 μm and the field flattener. Glass choice and coatings on these final two cold optics will provide the sharp cut off and long wavelength opacity needed to block the thermal background.

Impressively, due to the smaller field angle and the limited wavelength range, the design delivers images which

are better than the optical camera. In the spot diagram (Fig. 4) the indicated box size, 43 μm, represents 1 arcsec (2.3 pixels) while the 1.3 μm slits correspond to3.0 pixels. We point out, for any wavelength in z and J, 80–90% of the incident light falls within one pixel of the array.

4.2. Dispersing Optics

We design the grisms around the primary features we wish to detect: redshifted [OII] ($\lambda = 3727$ Å), the 4000 Å break and the G band ($\lambda = 4300$ Å). We consider the following to be a good compromise between wavelength coverage and resolution for the HAWAII array in LRS-J:

- one grism covering 0.85 to 1.1 μm at $R \sim 1900$ (1.0 arcsec slit)
- a second grism covering 1.09 to 1.35 μm (the entire J-band) also at $R \sim 2100$

The first grism covers redshifts $z = 1.3 - 1.5$ for all features, and when combined with the latter, the pair extends coverage to $z = 2.1$ for all three features. Also, since the (J − K) color of a galaxy is a good redshift discriminator, an educated assumption about the appropriate grism can be made prior to the observation.

Grism	Wavelength coverage	Fringe frequency	λc (μm)	R(1 arcsec)	t_{gel} (μm)	Δn	Bragg angle	Prism angle
VHG 1	0.87–1.10 μm	520 l/mm	0.985	1900	10	0.04	10.0	22.8
VHG 2	1.09–1.35 μm	450 l/mm	1.22	2100	12	0.05	15.0	24.5

Table 1. VH grism properties

Volume Holographic (VH) gratings have received a great deal of attention recently, primarily because of their high efficiency and the potential to design compact spectrographs of high resolution around them.[16] They utilize Bragg diffraction in a thin ($\sim 10\,\mu$m) dichromated gelatin layer with a 1-dimensional refractive index modulation. VH gratings have been used for many years in military applications, and there are currently several astronomical instruments under development which will utilize them.* While these instruments will have movable cameras to change the wavelength range and order being observed, it is possible to retrofit conventional grism spectrographs with VH grisms. We will adopt these grisms for the LRS-J for a number of reasons:

- potential of much higher efficiency (80–90%) than conventional grisms (typically 60–70% depending on the resolution),
- the wavelength range and resolution can be selected to match requirements, whereas few ruled grating masters exist for IR applications,
- they are available in large enough format for the LRS and cost no more than conventional grisms of similar size (the LRS-J will be the first time such large VH gratings have been used in an astronomical setting),
- and they do not suffer from the same limitations on maximum groove density. Conventional grisms are limited to groove frequencies of less than about 600 lines/mm, due to efficiency, whereas VH gratings can be made with more than 10 times that number.

The gratings are exposed in a thin layer of dichromated gelatin which is sandwiched between two optical quality BK7 flats. In order to use VH gratings as grisms, we sandwich the VH grating between two SF2 prisms designed to refract the light such that it is incident onto the grating at the Bragg angle. We will bond the prisms using Dow Corning QZ-3067 optical couplant, which we have successfully used on the multiplets in the LRS.

See Barden, et.al.[16] and Ralcon Development Lab[17] for details of the equations governing the design of VH gratings. We have used a semi-coupled wave calculation in Mathcad to calculate S and P polarization efficiencies for a number of gratings that fit our requirements for dispersion and wavelength coverage. The variables are the gelatin thickness (t_{gel} up to 20 μm), the modulation amplitude of the refractive index of the fringes ($\Delta n = 0.02$ to 0.1), in addition to the fringe frequency.

*OSIRIS for GranTeCan for example

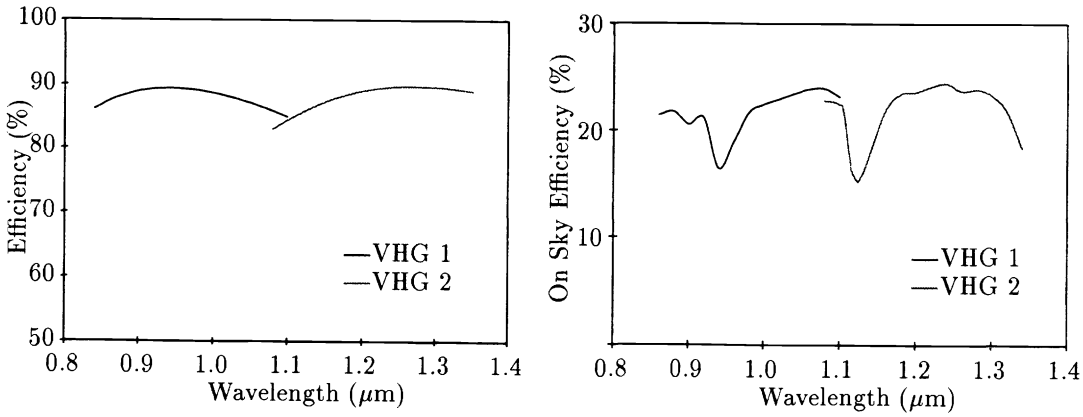

Figure 3. On the left is predicted VHG Efficiency. On the right is our predicted overall on sky efficiency of LRS-J. It is worth noting that in general predicted efficiencies of VH gratings are close to actual measured values.

5. MECHANICAL DESIGN

Our initial design is based on a closed cycle cryocooler; it is presented here, but we are still evaluating other configurations. Among those are a dual LN_2 dewar system, and a combination system based on our current cryocooler which could significantly increase the nitrogen hold time.

5.1. Thermal Design

Due to its compact size and cooling capabilities, we plan to use a CTI Cryogenics Cryodyne two-stage, closed-loop helium cooler for the camera s cryogenic system. The Model 22 refrigerator can typically provide 8 Watts of cooling at 85 K on its first stage, and 2 Watts of cooling at 30 K on its second stage. The first stage will be tied to a radiation shields inside the camera cryostat and the second stage will cool the cold arm leading to the detector. The temperature of the detector is tuned with the connection of braid between the second stage cooler and the cold block, and maintained by an internal heater.

The camera dewar will consist of a stainless steel cylindrical outer case. Steel is chosen to minimize thermal expansion focus changes (any residual will be taken out by focusing the collimator). The bottom of the cylinder will be closed, with feed-throughs for primary mirror adjusters, and the top will accommodate the pair of corrector lenses, the outer of which also serves as a vacuum window. A thin aluminum radiation shield will reside just inside the steel case, attached to the outer wall via three G10 insulating tabs. The shield, which serves the dual purpose of limiting the solid angle seen by the detector and limiting the thermal radiation load on cooling system, will be gold coated on the outside and painted flat black on the inside. We plan to use a special baked-on paint with an emissivity of 0.97-0.98, made by IITRI Research Institute that has previously been used in high vacuum systems. The cold arm leading from the second stage of the cryocooler to the detector will be surrounded by a second radiation shield, black on the outside and gold on the inside.

The temperature of the detector and cryocooler stages will be monitored with RTD (resistive thermometer detector) components, and heating resistors in the cold block will be used to raise the temperature to about 78K (a value that will be tuned for optimum QE/dark count). This temperature maintenance is identical to that used on our CCDs and will utilize a standard McDonald Observatory temperature controller. Copper braid will connect the second-stage head to the detector cold block, isolating the detector from vibration, and providing the thermal resistance in the closed loop cooling circuit. The temperature difference (50-60K) between the cold stage of the cryocooler and the cold block is similar to that used for the optical LRS cryostat, with a thermal link resistance of 40 K/W and a heater power of 0.7 W. We expect a similar heater power for the LRS-J cold block. Thermal load estimates for the system indicate that the Model 22 cooler will be adequate for our cooling requirements, even at a very conservative 300K (80 F):

An evacuated cryocamera is dictated to minimize obstruction and by the thermal background analysis above. The basic design is similar to the optical camera (Fig. 4), but the design is probably simpler than for the optical CCD cryostat, due to the harsh obscuration constraints applied to that system.

Radiation from steel outer case (300 K) to gold-coated radiation shield (200 K)	1.3 W
Radiation from gold-coated cold arm shield (200 K) to gold-coated cold arm (20 K)	0.01 W
Radiation from corrector lens (300 K) to black-painted cold arm shield (200 K)	3.8 W
Radiation reflected by primary mirror (300 K) to black-painted cold arm shield (200 K)	0.9 W
Gas conduction from outer wall to radiation shield (10^{-5} torr)	0.04 W
Conduction through stainless steel vanes on detector mount and signal wiring	0.6 W
Conduction through three G10 mounts on radiation shield	0.5 W
Thermal heating from temperature controller to detector	< 1 W
Total on 1st Stage (8 W at 85 K capacity)	< 7.1 W
Total on 2nd Stage (2 W at 30 K capacity)	1.01 W

Table 2. Estimated thermal load on cooling system

- Only the detector, field lens, blocking filter, and radiation shields will be cooled because the camera accepts thermal emission from the $\epsilon = 1$ warm spectrograph, so cooling the mirror or corrector lenses is pointless.
- So, we can use three feed-throughs to align the mirror without worrying about heat conduction.
- The corrector lenses can be any material with an efficient multi-layer AR coating since their emissivity will not matter. The cold shielding restricts the solid angle seen by the detector.
- Thermal cooling of the corrector lenses by radiation to the cold surfaces will not result in condensation on the outer element because both elements are tied to the ambient temperature through the outer casing. Additionally, the interior of the LRS is purged with dry air.

5.2. Physical Layout

Preliminary layouts indicate that a detector mount and cold block scheme similar to that for the CCD can be used for the HAWAII array. The detector head package will be suspended within the camera body with four stainless steel vanes tied to the cryostat wall. The cold head of the CTI Model 22 cryocooler and its radiation shield will protrude into the beam and a copper braid will link it to the detector cold block.

The fast mirror of the camera will be Zerodur^{TM}, and can be aligned to the detector in tip, tilt, and piston with three feed throughs at the back of the camera body. This element need not be cooled, so these adjusters will not affect the heat load. The detector package will be used as the alignment reference, so it need not be adjustable. The two large corrector lenses need only be aligned to ~ 0.5 mm to meet the image quality requirements, which is trivially done with machining tolerances. As stated above, the optical design is insensitive to alignment errors and we expect the IR camera to be as easy to set up as the optical one.

With the exception of flexure in the dewar window, all other known mechanical difficulties have been solved during the commissioning of the LRS. We have now demonstrated that instrumental flexure is not an issue within the time of a single track, furthermore the LRS-J has no moving components since the camera shutter is part of the LRS collimator. The one major mechanical difference, evacuation of the camera in the LRS-J, will result in moderate flexure in the dewar window. The pressure differential on this window motivates, to an extent, our choice of SF10 as its optical glass. We intend to use finite element analysis software to model the flexure of this lens. We will then specify the optic such that it has the desired shape under the one-atmosphere pressure differential.

6. ELECTRONICS

As all hardware control systems of the LRS are currently in place and working, the LRS-J camera readout electronics are the only control component not yet built. We divide the system into two components: the array header board, which we will design and manufacture, and the readout electronics, which we may purchase.

HAWAII arrays are straight forward to run (compared to CCDs), having 4 outputs and readout rates of 1 Mpxl/second/output (0.25 sec to read the array).[18] Electronically, they are quite similar to the familiar NICMOS3 arrays, also fabricated by Rockwell. The major difference being a line reset on the HAWAII arrays vs. a pixel reset on

the older NICMOS3 arrays. This difference reduces the read noise of a pixel to a mere $6\,e^-$ (with double-correlated sampling). Designing a control system from the ground up is a daunting task, so we are considering two alternative options. The first and most desirable option is to design a module which would allow us to integrate this array with McDonald Observatory's current detector controllers. The second option, which will require new undeveloped software, is to purchase a commercial system. In either case, header electronics will need to be custom designed and built in house.

6.1. Header Electronics

As we already have a custom NICMOS3 system in place at McDonald (ROKCAM[19]), we are already familiar with some of design requirements of an array similar to the HAWAII. Other than the array itself, the LRS-J header board will be populated completely with passive components. The header board will, for a fully working scientific array, require no more than 13 separate filter circuits, each of which will consist of two tantalum capacitors and a single precision resistor. Precision resistors are desirable because of their relative stability with changing temperature. With high charge density components like tantalum capacitors, it should be possible to design a board such that all passive components are on the opposite side from the detector. We would like to keep the header board small enough that it does not add to the central obstruction.

6.2. Readout Electronics

The readout electronics are significantly more complex, but with ROKCAM we have a system that can put us on line as soon as the camera hardware is completed. The differing reset requirements of the HAWAII array amount to a microcode modification in the ROKCAM system. Since the ROKCAM electronics are much slower, this is not the optimal solution, but it is guaranteed to get us online with 6 s readouts soon.

With this system as a backup, we can consider an optimum design for the HAWAII array. At this point we are considering a unit which attaches to the LRS-J which we call the penthouse, this unit will house four independent preamplifier circuits (one for each quadrant), all necessary power supplies, and an analog multiplexer. This system could potentially interface to McDonald's next generation CCD controller, which will already be in place controlling the LRS CCD. This system is capable of 1 Mpxl/s readouts which is well within the limitations of the array itself.

7. SUMMARY

The optical LRS achieves peak efficiencies around 600 nm of 20 to 25% on the sky depending on the resolution. The model for the LRS has been borne out by 6 months of observations. LRS-J will have a predicted peak efficiency of over 20%, since the increased VHG efficiency counteracts the decreased detector QE (around 50%) (Fig. 3). This compares to only a few percent for the optical LRS for $R \sim 1000$ at 900 nm, dominated by the low CCD QE. Clearly the LRS-Jrepresents a dynamic improvement in sensitivity over the optical LRS in the region beyond 900 nm.

ACKNOWLEDGMENTS

The authors would like to acknowledge the invaluable work by F. J. Cobos and C. Tejada on the original LRS optical design. It served as a basis for the optical design of the LRS-J camera. Furthermore, we would like to especially thank C. Tejada for optimizing the LRS-J optical design. We would also like to acknowledge the help of K. L. Thompson in helping us to determine and optimal resolution for the LRS-J. Finally we would like to thank P. J. MacQueen for many discussions on electronics design and the internals of the new McDonald CCD controller.

REFERENCES

1. T. G. Barnes III, M. T. Adams, J. A. Booth, M. E. Cornell, N. I. Gaffney, J. R. Fowler, G. J. Hill, C. E. Nance, F. Piche, L. W. Ramsey, R. L. Ricklefs, W. J. Spiesman, and T. Worthington, "Commissioning experience with the 9.2-m Hobby-Eberly telescope," in *Telescope Structures, Enclosures, Controls, Assembly/Integration/Validation, and Commissioning*, T. A. Sebring and T. Andersen, eds., *Proc. SPIE* **4004**, submitted.
2. G. J. Hill, H. E. Nicklas, P. J. MacQueen, C. Tejada, F. J. Cobos Duenas, and W. Mitsch, "Hobby-Eberly Telescope low-resolution spectrograph," in *Opical Astronomical Instrumentation*, S. D'Odorico, ed., *Proc. SPIE* **3355**, pp. 375–386, July 1998.

3. R. R. Joyce, K. H. Hinkle, M. R. Meyer, and M. F. Skrutskie, "Infrared astronomical spectroscopy with a non-cryogenic spectrograph," in *Infrared Astronomical Instrumentation*, A. M. Fowler, ed., *Proc. SPIE* **3354**, pp. 741–749, Mar. 1998.
4. R. Dallier and J. G. Cuby, "Non-cooled near infrared spectroscopy," in *Infrared Astronomical Instrumentation*, A. M. Fowler, ed., *Proc. SPIE* **3354**, pp. 833–844, Mar. 1998.
5. G. J. Hill, "Science with the hobby-eberly spectroscopic survey telescope," in *Wide Field Spectroscopy*, S. J. Maddox and A. Aragon-Salamanca, eds., p. 49, World Scientific, Singapore, 1995.
6. L. W. Ramsey, M. T. Adams, T. G. Barnes, J. A. Booth, M. E. Cornell, J. R. Fowler, N. I. Gaffney, J. W. Glaspey, J. M. Good, G. J. Hill, P. W. Kelton, V. L. Krabbendam, L. Long, P. J. MacQueen, F. B. Ray, R. L. Ricklefs, J. Sage, T. A. Sebring, W. J. Spiesman, and M. Steiner, "Early performance and present status of the Hobby-Eberly Telescope," in *Advanced Technology Optical/IR Telescopes VI*, L. M. Stepp, ed., *Proc. SPIE* **3352**, pp. 34–42, Aug. 1998.
7. S. D. Horner, L. G. Engel, and L. W. Ramsey, "Hobby-Eberly Telescope medium-resolution spectrograph and fiber instrument feed," in *Opical Astronomical Instrumentation*, S. D'Odorico, ed., *Proc. SPIE* **3355**, p. 399, July 1998.
8. R. G. Tull, "High-resolution fiber-coupled spectrograph of the Hobby-Eberly Telescope," in *Opical Astronomical Instrumentation*, S. D'Odorico, ed., *Proc. SPIE* **3355**, p. 387, July 1998.
9. F. J. Cobos Duenas, C. Tejada, G. J. Hill, and F. G. Perez, "Hobby-Eberly Telescope low-resolution spectrograph: optical design," in *Opical Astronomical Instrumentation*, S. D'Odorico, ed., *Proc. SPIE* **3355**, pp. 424–432, July 1998.
10. G. J. Hill, H. E. Nicklas, P. J. MacQueen, W. Mitsch, W. Wellem, W. Altmann, G. L. Wesley, and F. B. Ray, "Hobby-Eberly Telescope low-resolution spectrograph: mechanical design," in *Opical Astronomical Instrumentation*, S. D'Odorico, ed., *Proc. SPIE* **3355**, pp. 433–443, July 1998.
11. M. J. Wolf, G. J. Hill, W. Mitsch, F. V. Hessman, and W. Altmann, "Multiobject spectroscopy on the Hobby-Eberly telescope low-resolution spectrograph," in *Optical and IR Telescope Instrumentation and Detectors*, M. Iye and A. F. Moorwood, eds., *Proc. SPIE* **4008**, submitted.
12. T. Maihara, F. Iwamuro, T. Yamashita, D. N. B. Hall, L. L. Cowie, A. T. Tokunaga, and A. Pickels, "Observations of the OH airglow emission," *PASP* **105**, p. 940, 1993.
13. K. L. Thompson, "A near-infrared spectrometer optimized for an adaptive optics system," *Mon. Not. RAS* **303**, p. 15, 1999.
14. C. D. Mackay, M. G. Beckett, R. G. McMahon, I. R. Parry, F. Piche, K. A. Ennico, M. A. Kenworthy, R. S. Ellis, and A. Aragon-Salamanca, "Infrared imaging and spectroscopy with hawaii and picnic arrays," in *Infrared Astronomical Instrumentation*, A. M. Fowler, ed., *Proc. SPIE* **3354**, pp. 14–23, Mar. 1998.
15. L. J. Kozlowski, K. Vural, S. A. Cabelli, A. C. Chen, D. E. Cooper, G. L. Bostrup, C. Cabelli, K.-W. Hodapp, D. N. Hall, and W. E. Kleinhans, "HgCdTe 2048^2 FPA for infrared astronomy: Development status," in *Infrared Astronomical Instrumentation*, A. M. Fowler, ed., *Proc. SPIE* **3354**, pp. 66–76, Mar. 1998.
16. S. C. Barden, D. G. Sawyer, and R. K. Honeycutt, "Volume-phase holographic gratings and their potential for astronomical applications," *Proc. SPIE* **3355**, p. 866, July 1998.
17. Ralcon Development Labs, *http://www.xmission.com.*
18. Rockwell Science Center, *http://www.rsc.rockwell.com/mct_fpa/Hawaii/hawaii.html.*
19. M. Kaiser and G. Hill, "Near infrared observations of 3c208.1," in *Infrared Astronomy with Arrays: the Next Generation*, I. McLean, ed., Kluwer, Dordrecht, 1994.
20. G. J. Hill, "Hobby-Eberly telescope: instrumentation and current performance," in *Optical and IR Telescope Instrumentation and Detectors*, M. Iye and A. F. Moorwood, eds., *Proc. SPIE* **4008**, submitted.

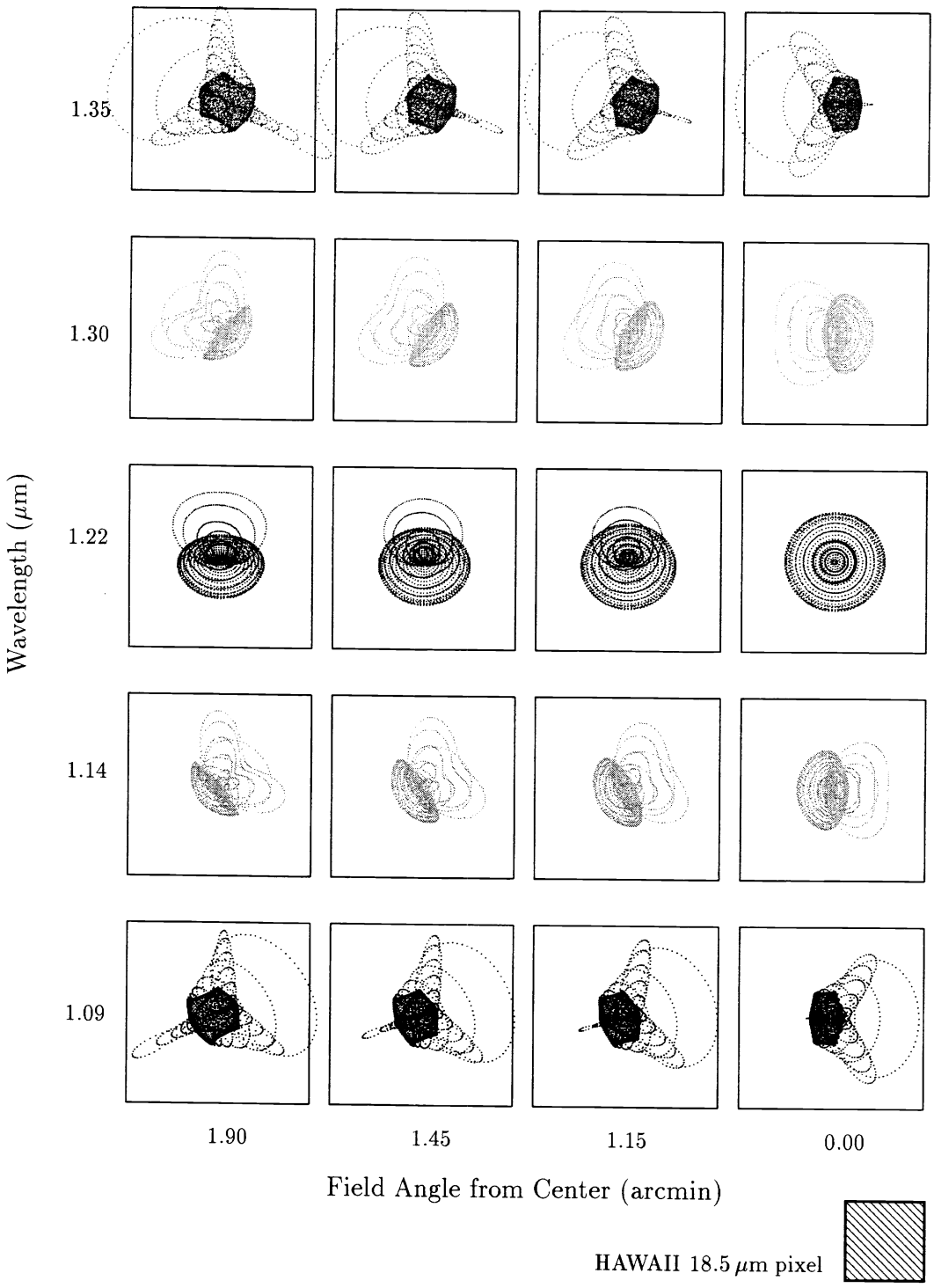

Figure 4. Spot diagram at the plane of the HAWAII array. Field angle is plotted on the horizontal axis while wavelength is on the vertical axis. The box size is 1.0 arcsec, and the wavelengths correspond to the range for VHG 2.